Three-Phase Inverter with Direct Torque Control for a Brushless DC Motor

Sirichai Dangeam†, Non-member

ABSTRACT

This paper presents the implementation of a three-leg voltage source inverter fed by a brushless DC motor. The open-loop speed control with direct torque is employed in this motor. The rotation of the motor is controlled by using an optimal voltage vector which is related to the calculation of stator flux and electromechanical torque. The experimental results show that this system has greater capability to reduce spike and ripple on the voltage, current, stator flux, and electromechanical torque than the conventional speed controller which feeds the voltage vector from the hall-effect sensors.

Keywords: Three-Phase Inverter, Direct Torque Control, Brushless DC Motor

1. INTRODUCTION

In recent years, the adjustable speed drive has been growing in efficiency through advanced technology. Although DC motor performs satisfactorily in terms of speed and torque control, the frequent maintenance of the commutator and brushes are a major disadvantage. Permanent Magnet Synchronous Motor (PMSM) and Brushless DC Motor (BLDC) have been developed to resolve the maintenance problem encountered with the DC motor by using solid-state switches such as IGBT/MOSFET. However, PMSM and BLDC must be used with an inverter to control the speed. Besides, the construction of these motors is different. The PMSM is a cylindrical type of construction which means the stator is wound with distributed winding and the back electromotive force (back emf.) consists of a sinusoidal waveform. Whereas the BLDC is a salient-pole type. The stator is wound with concentrated windings and the back emf. has a trapezoidal waveform [1, 2]. Both motors are popularly used in industry application and especially in electric vehicle drives since they are lightweight, have eminent power density, high efficiency, and simple to control. The PMSM is mostly used in passenger cars and trucks due to its smooth torque and small size. Whereas the BLDC is mostly used in electric bikes or motorcycles and mini electric cars because of its high starting torque [3]. However, this paper essentially discusses only the BLDC because it is simple to control by using a voltage switch suitable for the rotor flux position; so-called conventional control (CC) [1–3]. Nevertheless, the spikes on its current waveform need to be improved.

The direct torque control (DTC) strategy was first proposed by Takahashi *et al.* [4, 5] and Depenbrock [6] for induction motor drives. The principle is based on the stator flux and electromechanical torque control using optimal voltage vectors with no speed transducer on the motor shaft. Due to its high performing torque and fast response, the DTC is frequently used with motor drives. However, the main advantages of the classical DTC method are its big ripple torque, drop in stator flux, variable switching frequency, high noise level at low speed, and so on [7].

This paper proposes the implementation of a direct torque control strategy to control the three-phase BLDC fed by a three-leg voltage source inverter (VSI) to achieve the required result. Therefore, the experimental results will show the essential differences between the conventional control (CC) and DTC for the BLDC drive.

2. BRUSHLESS DC MOTOR

2.1 Construction

The BLDC has two parts: armature winding and a permanent magnet. Mostly, the armature winding is performed on the salient-pole core at the stator with the permanent magnets installed in the rotor part. There are three types of BLDC: radial, in-wheel, and axial. However, only the axial f BLDC is used in this research. In addition, three hall sensors are installed in the stator winding slots, placed 120 electrical degrees apart. These hall sensors are used to detect the position of the magnetic poles on the rotor.

2.2 Three-Phase Inverter and Conventional Commutation

The key to controlling the speed of the BLDC is the three-leg voltage source inverter (3-Leg VSI). To achieve this, six switches (Q_1–Q_6) are connected in the circuits as shown in Fig. 1. However, the rotor shaft is moved by synchronizing it with the synchronous speed of the stator flux, which must be energized and related to the rotor magnetic pole at the stator pole face.

The main principle for conventional control (CC)

Manuscript received on September 9, 2021; revised on October 23, 2021; accepted on November 11, 2021. This paper was recommended by Associate Editor Yuttana Kumsuwan.

The author is with the Department of Electrical Engineering, Faculty of Engineering, Rajamangala University of Technology Thanyaburi, Thailand.

†Corresponding author: sirichai.d@en.rmutt.ac.th

Digital Object Identifier: 10.37936/ecti-eec.2022201.246118

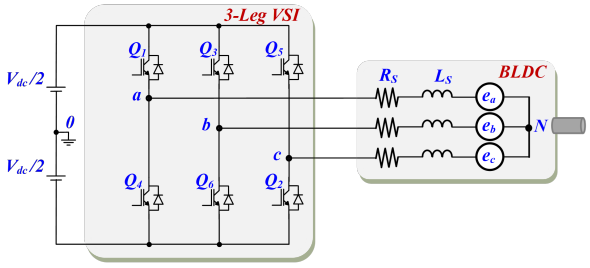

Fig. 1: *Three-phase inverter for the BLDC drive system.*

Table 1: *Switching table for conventional control.*

Sector	Ha	Hb	Hc	Q_1	Q_3	Q_5	Q_4	Q_6	Q_2	v_{a0}	v_{b0}	v_{c0}
1	1	0	0	1	0	0	0	0	1	$V_{dc}/2$	0	$-V_{dc}/2$
2	1	1	0	0	1	0	0	0	1	0	$V_{dc}/2$	$-V_{dc}/2$
3	0	1	0	0	1	0	1	0	0	$-V_{dc}/2$	$V_{dc}/2$	0
4	0	1	1	0	0	1	1	0	0	$-V_{dc}/2$	0	$V_{dc}/2$
5	0	0	1	0	0	1	0	1	0	0	$-V_{dc}/2$	$V_{dc}/2$
6	1	0	1	1	0	0	0	1	0	$V_{dc}/2$	$-V_{dc}/2$	0

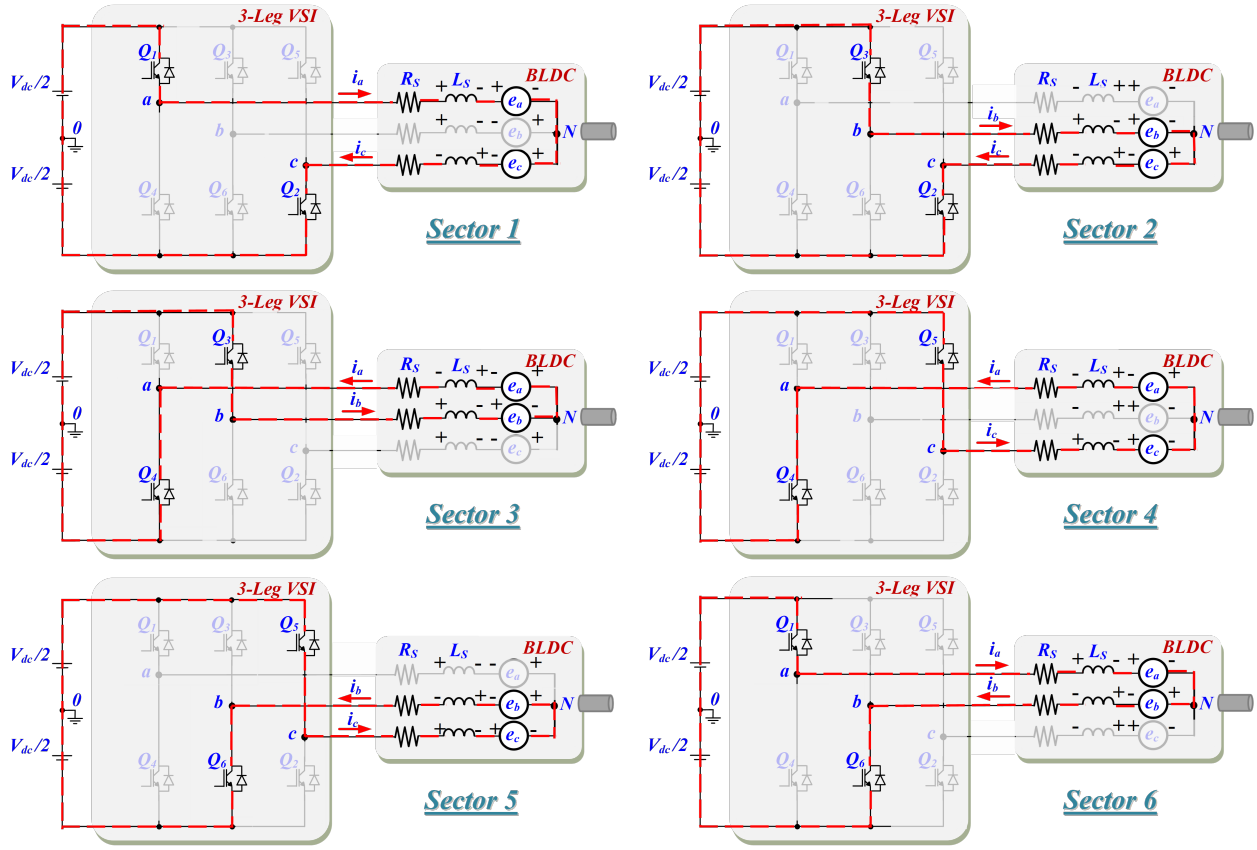

Fig. 2: *Circuit operation during each sector in Table 1.*

of the BLDC controllers involves measuring the rotor magnetic flux with three hall-effect sensors to enable the processor of the conventional controller to determine the optimal pattern for energizing the magnetic flux of the stator winding and attracting it to the permanent magnet on the rotor. Table 1 shows the pattern for each switch and their relationship to the six sectors in the rotation. However, it can be observed that each sector in Table 1 has only two switches which are conducted (as shown by logic "1") and each switch controls each leg of the inverter. Assuming that the sector is 3, according to Table 1, switches Q_3 and Q_4 are conducted. Therefore, the stator current in Fig. 2 flows through only two stator windings from phase *b*. For all sectors, the switching sequence can be commutated by Q_1Q_2, Q_3Q_2, Q_3Q_4, Q_5Q_4, Q_5Q_6, Q_1Q_6, and Q_1Q_2, respectively. The directions of the current flow through each phase of the motor winding for all sectors are shown in Fig. 2.

Fig. 3 shows the results of each phase of the current waveforms, back emfs., and hall-effect sensors by relating to each sector and gate drive signals. Where $\Phi_{a,b,c}$ represents the variation of the back emf. during the turnoff period for all switches in a phase-leg.

2.3 Mathematical Models

Due to its construction, the BLDC can transform into mathematical models in accordance with Fig. 2 as follows:

$$v_a = R_S i_a + L_S \frac{di_a}{dt} + e_a \tag{1}$$

$$v_b = R_S i_b + L_S \frac{di_b}{dt} + e_b \tag{2}$$

$$v_c = R_S i_c + L_S \frac{di_c}{dt} + e_c \tag{3}$$

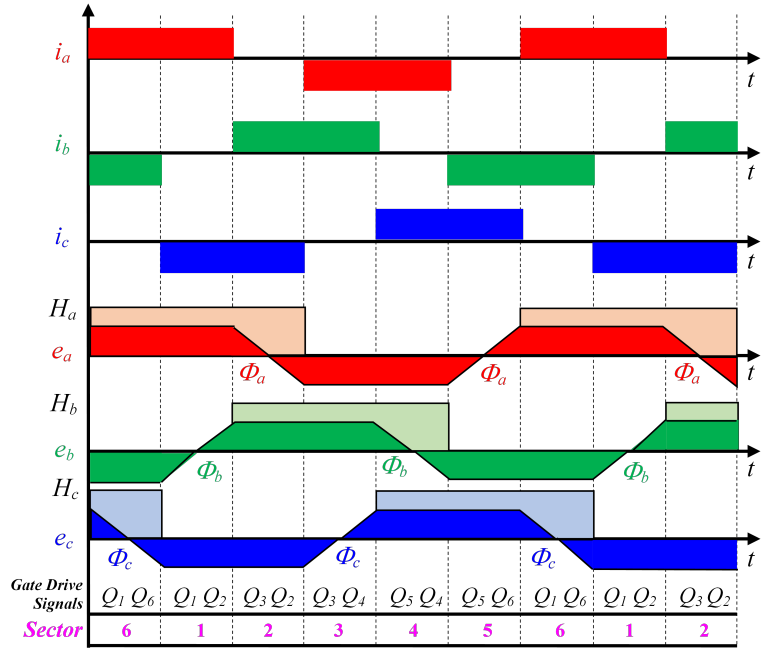

Fig. 3: *Current and back emf. waveforms for the BLDC drive system.*

$$e_a = K_W f(\theta_e)\omega \tag{4}$$

$$e_b = K_W f(\theta_e - \frac{2\pi}{3})\omega \tag{5}$$

$$e_c = K_W f(\theta_e + \frac{2\pi}{3})\omega \tag{6}$$

$$T_e = \frac{P}{2\omega}(e_a i_a + e_b i_b + e_c i_c) \tag{7}$$

where $v_{a,b,c}$ represent the motor terminal voltages of phase a, b, and c, respectively; $i_{a,b,c}$ are the motor currents of phase a, b, and c, respectively; $e_{a,b,c}$ are the motor back emfs. of phase a, b, and c, respectively; K_W is the constant of phase back emf.; θ_e is the electrical rotor angle; ω is the rotor angular speed; L_S is the stator inductance; R_S is the stator resistance; P represents the total motor poles; and T_e is the electromagnetic torque.

2.4 Simulation of Conventional Control

To analyze the performance of the BLDC speed control with the conventional control, the voltage, current, stator flux linkage, and electromechanical torque are transformed in α axis and β axis as:

$$\begin{bmatrix} v_\alpha \\ v_\beta \\ v_0 \end{bmatrix} = \frac{2}{3}\begin{bmatrix} 1 & -\frac{1}{2} & -\frac{1}{2} \\ 0 & \frac{\sqrt{3}}{2} & -\frac{\sqrt{3}}{2} \\ 1 & 1 & 1 \end{bmatrix}\begin{bmatrix} v_a \\ v_b \\ v_c \end{bmatrix} \tag{8}$$

$$\begin{bmatrix} i_\alpha \\ i_\beta \\ i_0 \end{bmatrix} = \frac{2}{3}\begin{bmatrix} 1 & -\frac{1}{2} & -\frac{1}{2} \\ 0 & \frac{\sqrt{3}}{2} & -\frac{\sqrt{3}}{2} \\ 1 & 1 & 1 \end{bmatrix}\begin{bmatrix} i_a \\ i_b \\ i_c \end{bmatrix} \tag{9}$$

$$\overline{\lambda_\alpha}(t) = \int_{t_0}^{t_n}\left[\overline{v_\alpha}(t) - R_S\overline{i_\alpha}(t)\right]dt \tag{10}$$

$$\overline{\lambda_\beta}(t) = \int_{t_0}^{t_n}\left[\overline{v_\beta}(t) - R_S\overline{i_\beta}(t)\right]dt \tag{11}$$

$$\left|\overline{\lambda_S}(t)\right| = \sqrt{(\lambda_\alpha^2(t) + \lambda_\beta^2(t))} \tag{12}$$

$$T_e(t) = \frac{3P}{2}\left(\lambda_\alpha(t)\cdot i_\beta(t) - \lambda_\beta(t)\cdot i_\alpha(t)\right) \tag{13}$$

where v_α and v_β are the stator terminal voltages in the α-axis and β-axis stator, respectively; i_α and i_β are the α-axis and β-axis stator currents, respectively; and λ_α and λ_β are the α-axis and β-axis stator flux linkages, respectively.

However, estimation of the two-phase stator flux linkage for the stationary reference frame in Eqs. (10) and (11) is considered to be ideal, despite the parameter variations for stator resistance from temperature during low-speed operation.

Fig. 4 shows the waveforms using the simulation program for the BLDC drive system with conventional control. The BLDC parameters for simulation with conventional control are 3 kW, 48 V, 4 poles, $R_S = 0.02\,\Omega$, $L_S = 73\,\mu$H. However, the simulation results in Fig. 4 differ from the waveform in Fig. 3, in that the simulation line-to-line voltages contain some spikes. These spikes come from the commutation of the phase current to zero while the inductive voltages ($L_S \cdot di_{a,b,c}/dt$ voltages in Eqs. (1)–(3)) subsequently occur during this time following these equations.

On the other hand, during the sector changing process, sector 2 change into sector 3. The line voltage v_{ca} changes the polarity from a negative cycle into a positive. However, the inductive voltage during this time remains

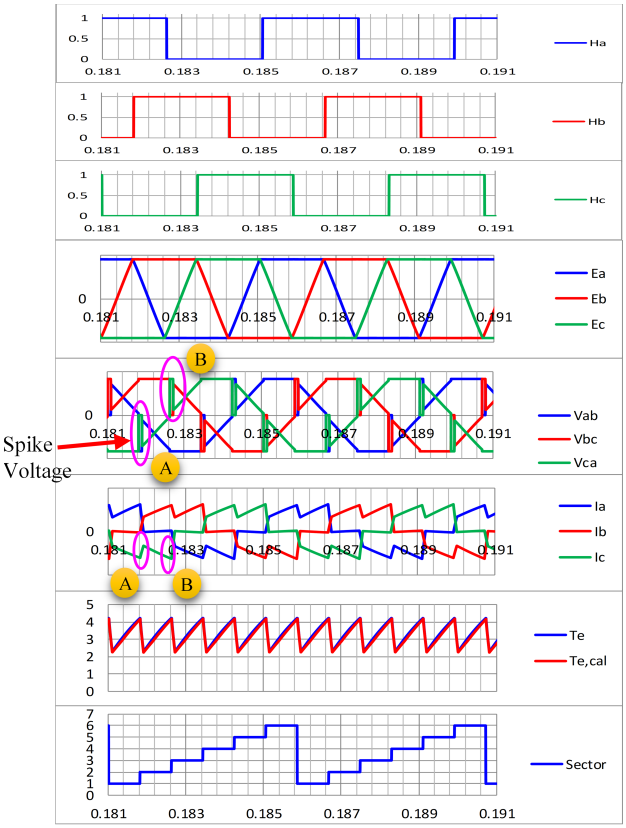

Fig. 4: *Simulation results of the BLDC drive system with conventional control.*

positive and reinforces to immediately reach the high line voltage v_{ca} at point "B" for a while. Meanwhile, the stator current i_c at point "B" is increased as the line voltage v_{ca} increases. Therefore, the inductive voltage can cause stator current ripple. Furthermore, like the stator current, the electromechanical torque also has some ripples.

3. DIRECT TORQUE CONTROL PRINCIPLE

Fig. 5 shows the proposed BLDC open-loop speed control system with direct torque control (DTC). The core strategies of DTC essentially control the stator flux linkage and electromechanical torque by feeding the optimal voltage vector according to the sector of the stator flux at that time [4–8]. The principles of the DTC strategy are described below.

Following to the equation of the stator flux linkage, $\lambda_{\alpha\beta}$ can be written as

$$\overline{\lambda_{\alpha\beta}}(t) = \int_{t_o}^{t_n} \left[\overline{v_{\alpha\beta}}(t) - R_S \overline{i_{\alpha\beta}}(t)\right] dt. \tag{14}$$

Considering Eq. (14), although the terminal voltage is quite low, the stator resistance voltage drop is very small when the BLDC is running at high speed. The stator flux linkage in Eq. (14) can then be modified as

$$\overline{\lambda_{\alpha\beta}}(t) = \overline{v_{\alpha\beta}}(t)\Delta t + \overline{\lambda_{\alpha\beta}}(t_0)\Big|_{\Delta t = t_n - t_0}. \tag{15}$$

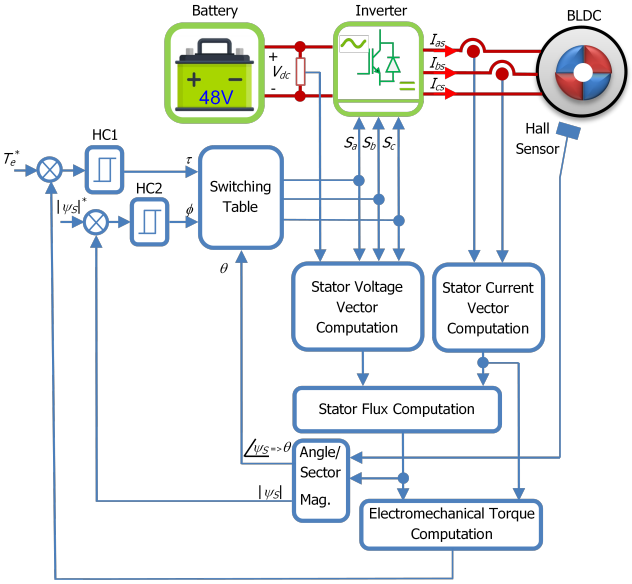

Fig. 5: *The proposed BLDC drive system with direct torque control.*

Table 2: *Switching table for direct torque control.*

ϕ	τ	$\theta(N)$					
		$\theta(1)$	$\theta(2)$	$\theta(3)$	$\theta(4)$	$\theta(5)$	$\theta(6)$
$\phi = 1$	$\tau = 1$	V_6	V_2	V_3	V_1	V_5	V_4
	$\tau = 0$	V_7	V_0	V_7	V_0	V_7	V_0
	$\tau = -1$	V_5	V_4	V_6	V_2	V_3	V_1
$\phi = 0$	$\tau = 1$	V_2	V_3	V_1	V_5	V_4	V_6
	$\tau = 0$	V_0	V_7	V_0	V_7	V_0	V_7
	$\tau = -1$	V_1	V_5	V_4	V_6	V_2	V_3

The electromechanical torque, T_e of BLDC, can be expressed as

$$T_e(t) = \frac{3P}{2}\left(\lambda_\alpha(t) i_\beta(t) - \lambda_\beta(t) i_\alpha(t)\right). \tag{16}$$

After calculating the stator flux linkage and electromechanical torque, these variables are sent to the hysteresis controllers to determine the errors in the stator flux linkage and electromechanical torque references.

The three-level hysteresis controller (HC1) is used to control the electromechanical torque and direction of the rotating motor. Meanwhile, the two-level hysteresis controller (HC2) is used to control the stator flux linkage.

Fig. 6 shows the trajectories of the stator flux linkage and the electromechanical torque. The stator flux linkage is controlled under the hysteresis band, selecting the six-voltage vectors ($V_1 - V_6$) shown in Fig. 6(a) and forcing the rotation of the stator flux trajectory until it is almost circular. It can be observed that bits 1 or 0 behind the voltage vectors ($V_1 - V_6$) mean that the upper or lower switch on each leg of the 3-leg VSI are active, respectively. Furthermore, the length of each voltage vector in Fig. 6(a) is not equal because of the hysteresis control behavior. Consequently, it can cause a variation in the switching frequency and switching loss

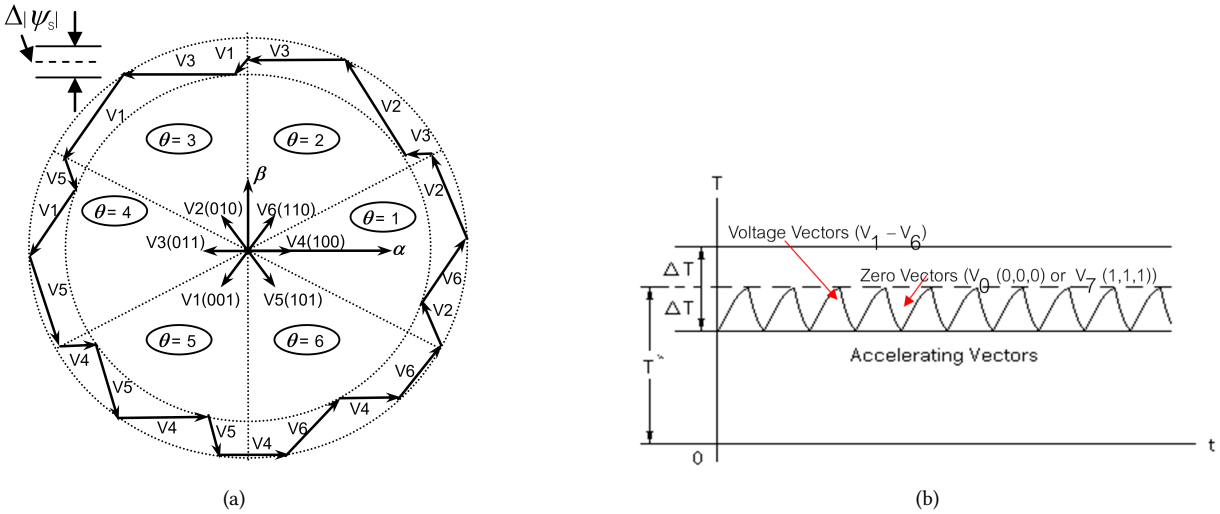

(a) (b)

Fig. 6: *Locus of (a) the calculated stator flux linkage and (b) the calculated electromechanical torque.*

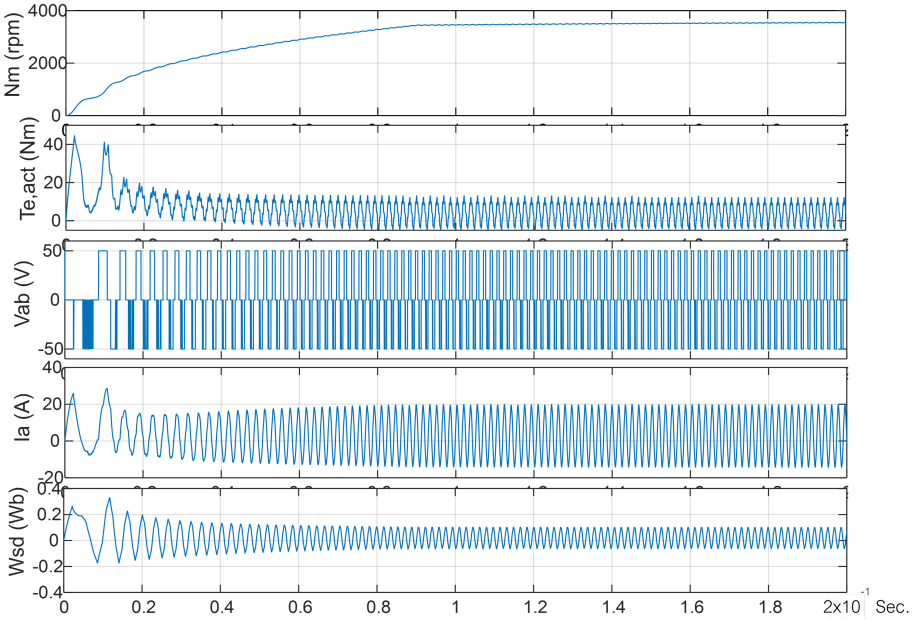

Fig. 7: *Simulation results of the BLDC drive system with direct torque control.*

for inverter devices. The electromechanical torque is controlled under the hysteresis band using the six-voltage vectors and two zero voltages (V_0 and V_7) as shown in Fig. 6(b). Each time, the optimal voltage vector is selected from Table 2 by considering the variables of flux, torque, and sector, respectively.

The error output of HC1 generates the logic for the torque variable (τ). When the magnitude of the electromechanical torque is greater than the higher hysteresis band, HC1 generates the logic "0". While the magnitude of the electromechanical torque is lower than the lower hysteresis band, HC1 generates the logic "1". However, logic "1" is used for the forward direction, and otherwise, logic "−1" may be used for the reverse direction.

The error output of HC2 generates the logic for the flux variable (ϕ). When the magnitude of the stator flux linkage is less than the lower hysteresis band, HC2 generates logic "1". When the magnitude of the stator flux linkage is greater than the higher hysteresis band, HC2 generates logic "0".

However, the size of the hysteresis band affects the ripple on the stator flux linkage and electromechanical torque. When the size of the hysteresis band is tiny, the ripple on the signals is very low, but the switching frequency is very high. Fortunately, the variation in switching frequency is satisfactorily reduced by the constant switching frequency operation of the PWM technique [7].

The sector variable (θ) determines the position of the stator flux. There are six sectors in the stator flux linkage, all ranging about 90 degrees apart as shown in Fig. 6(b).

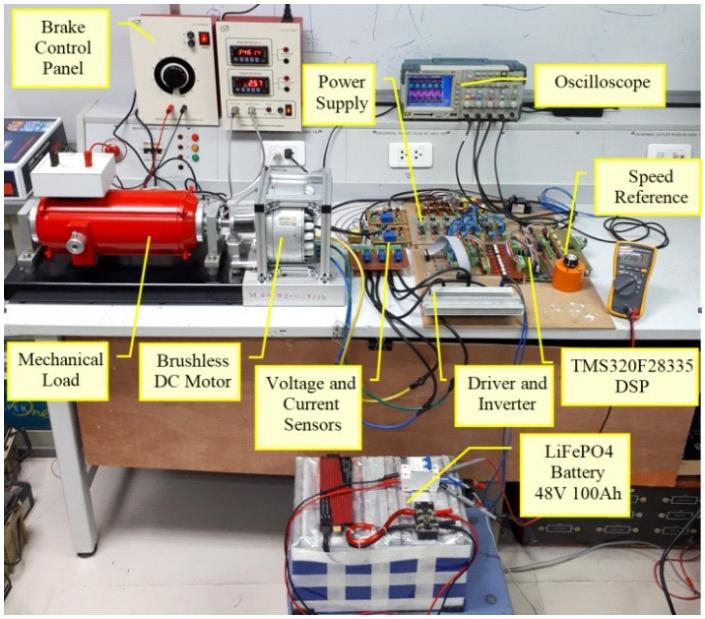

Fig. 8: *Proposed BLDC drive system.*

However, the stator and rotor flux angles of the BLDC must be controlled simultaneously. Hence, in this paper, three hall sensors are employed to track the rotor flux sector. Even though the accuracy of the hall sensor is quite low, at 60 degrees per step, the sector in the proposed DTC system needs to detect only six sectors (or 60 degrees per sector) and operate at high speed. The hall sensor is suitable for detecting the sector. In addition, the advantage of the hall sensor is its low cost.

The simulation results of the proposed BLDC drive system with the DTC are shown in Fig. 7. The proposed open-loop control system with DTC can control speed under load conditions. The stator current I_a, α-axis stator flux linkage W_{sd}, with DTC exhibits an almost sinusoidal waveform compared to the drive system with the CC. The simulation results confirm the capability of the DTC drive system prior to its implementation in real hardware.

4. EXPERIMENTAL RESULTS

Fig. 8 shows the implementation of the proposed BLDC drive system with DTC. The BLDC parameters are 3 kW, 48 V, 4 poles, $R_S = 0.02\,\Omega$, $L_S = 73\,\mu$H, while the flux and torque hysteresis band are set at 0.001. The switching frequency is 7.5 kHz and the DC bus voltage supplied by 48 V 100 Ah from a lithium iron phosphate battery (LiFePO4). The proposed open-loop speed drive system with DTC for BLDC in Fig. 8 is obtained by using Matlab/Simulink software for implementation on a TMS324F28335 digital signal processor.

Figs. 9 to 13 show the experiment results by comparing CC with DTC.

Fig. 9(a) demonstrates the spike voltage occurring during current commutation in each stator winding on the terminal voltage (or line-to-line voltage) waveforms with CC but DTC can suppress this spike voltage from the voltage waveform with two zero voltage vectors (V_0 and V_7). When using the zero voltage vectors, the storage energy from the inductive voltage in all windings can be reduced by forcing it to dissipate the energy at the motor winding. However, when comparing the terminal voltage spectrum in Fig. 9(b), the total harmonic distortion of the voltage waveform (THDv) in CC is quite severe with total harmonic distortion of 44.1472%. However, this is less than DTC which has a total harmonic distortion of 61.4122%. In addition, the DTC terminal voltage waveform looks like the typical industrial inverter PWM voltage.

Fig. 10(a) shows the high ripple of the current waveforms with CC. A high current ripple can damage the inverter switch, due to the changing rate of di/dt. Meanwhile, DTC can arrange the current waveform to be almost sinusoidal. The total harmonic distortion of the current waveform (THDi) of CC is quite distorted with a total harmonic distortion of 64.0909%. Meanwhile, the THDi of DTC is confirmed to have lower total harmonic distortion of 19.1816% as shown in Fig. 10(b).

Fig. 11 shows the calculated stator flux linkage and electromechanical torque. The CC has a linear line in the calculated stator flux, while DTC has some ripple on the line of the stator flux due to the system attempting to control the stator flux. It can be observed that for the calculated electromechanical torque, the CC controls both positive and negative torque with some degree of ripple. While DTC attempts to control only the positive torque as the reference and has more magnitude than CC with lower ripple on the torque.

Fig. 12 demonstrates the calculated stator flux linkage in the α-axis and β-axis along with the corresponding trajectory. The stator flux linkage waveforms are almost sinusoidal as shown in Fig. 12(a), while the stator flux linkage trajectory in Fig. 12(b) is nearly circular.

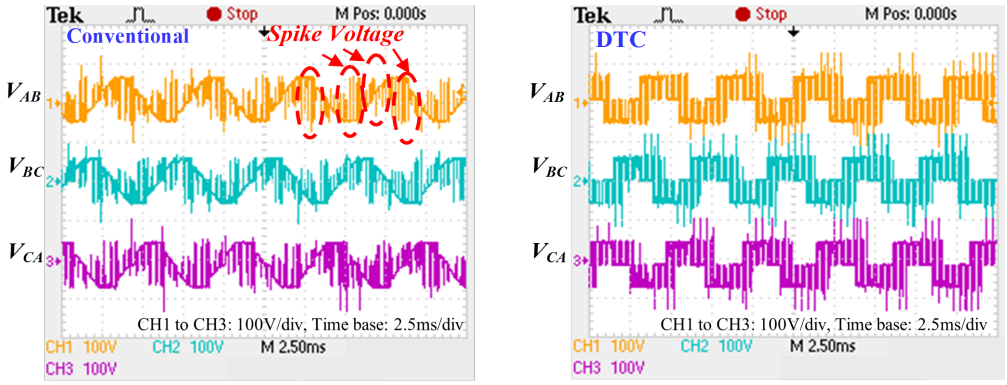

(a) Terminal voltage waveforms

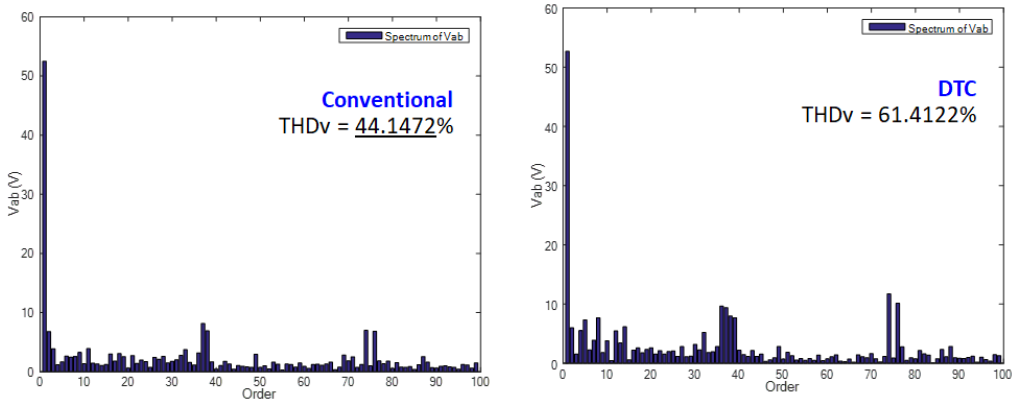

(b) Corresponding harmonic spectra of the measured terminal voltages

Fig. 9: *Terminal voltage comparison between conventional control and direct torque control.*

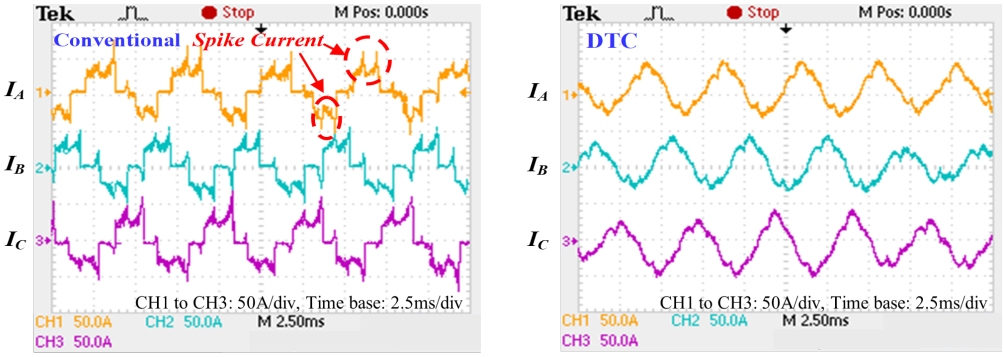

(a) Stator current waveforms

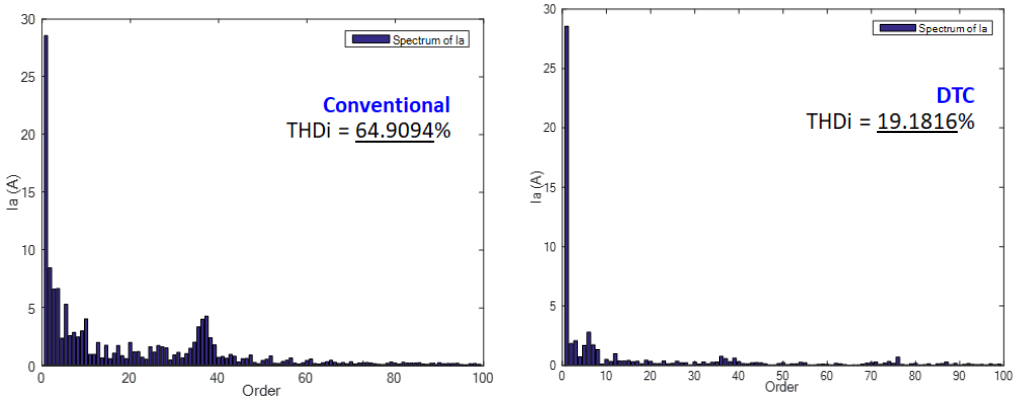

(b) Corresponding harmonic spectra of the measured stator currents

Fig. 10: *Stator current comparison between conventional control and direct torque control.*

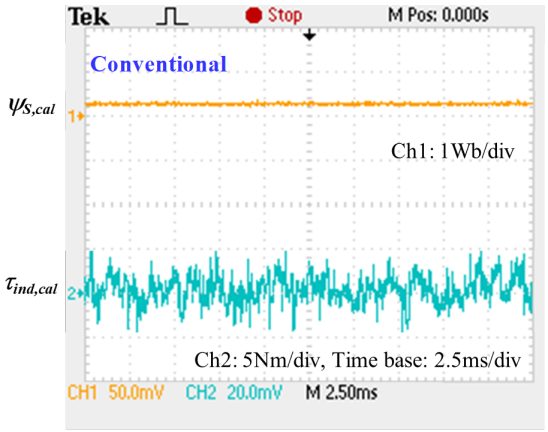

(a)

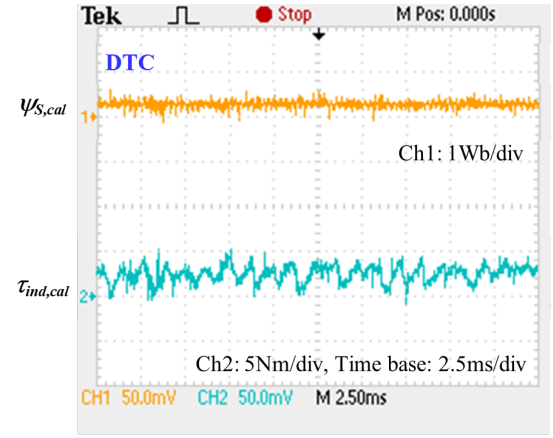

(b)

Fig. 11: *Calculated stator flux and electromechanical torque waveforms comparison between (a) conventional control and (b) direct torque control.*

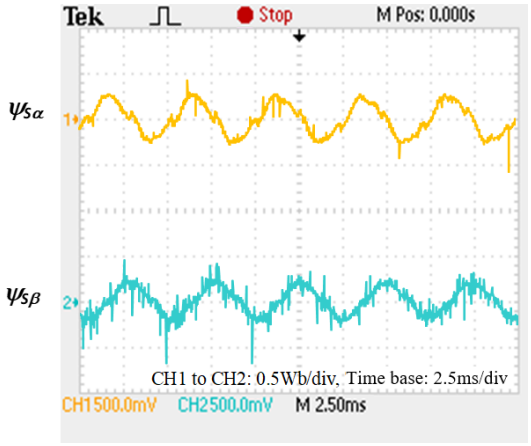

(a) Stator flux linkage in the α-axis and β-axis

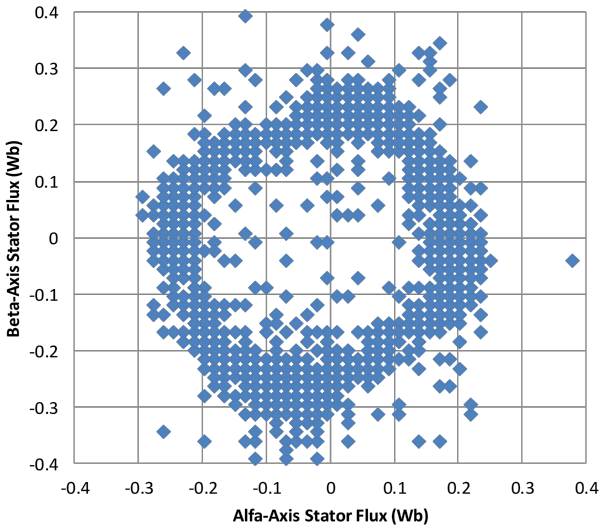

(b) Corresponding trajectory

Fig. 12: *The locus of the calculated stator flux linkage in the α-axis and β-axis with direct torque control.*

To analyze the dynamic performance of the open-loop speed control system with DTC shown in Fig. 13, the system has been tested under various conditions to observe the torque and speed response such as start-up, speed reversal, and so on.

Fig. 13(a) shows the no-load speed response during the start-up of the BLDC. For this test operation, the reference speed of BLDC is set at 1,000 rpm. The experimental results in Fig. 13(a) show the responses of an immediate step change from standstill to speed and the corresponding stator current waveform of the BLDC. The speed of BLDC reached the reference values within 250 ms. The proposed DTC system can control the BLDC start-up. It can be observed that the starting current is approximately equal to the steady state current due to the electromechanical torque loop control.

Fig. 13(b) shows the response to changing reference speed commands and reversing the speed direction with no-load. The proposed DTC drive system can control the shaft speed of the BLDC according to the reference speed commands with open-loop speed control. Fig. 13 (b) shows the multi-range speed response of the BLDC. The motor reference speed commands are set at 250 rpm in the reverse direction, 500 rpm and 1,000 rpm in the forward direction before finally stopping at the end. The BLDC shaft speed is controlled to rotate according to the speed reference commands. The acceleration and deceleration times during changes in the shaft speed of the BLDC are about 250 ms. The stator current during forward and reverse directions is almost the same due to the controlled electromagnetic torque.

It can be observed that when the shaft speed of the BLDC in both Figs. 13(a) and 13(b) is controlled by the speed command, it drops from 1,000 rpm then suddenly stops. There is a sudden drop from 1,000 rpm to negative values and a decay from negative speed to 0 rpm. This result occurs because of the no-load speed open-loop control behavior.

In the case of a step change under load conditions, Fig. 13(c) shows the responses of the shaft speed and stator currents of the BLDC when it is immediately

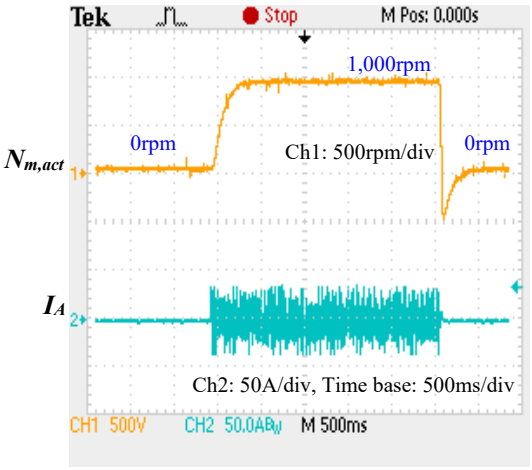

(a) Step speed change at different speeds

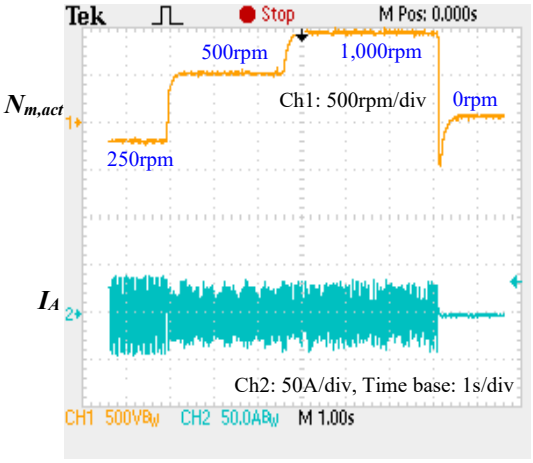

(b) Speed responses at different speeds and directions

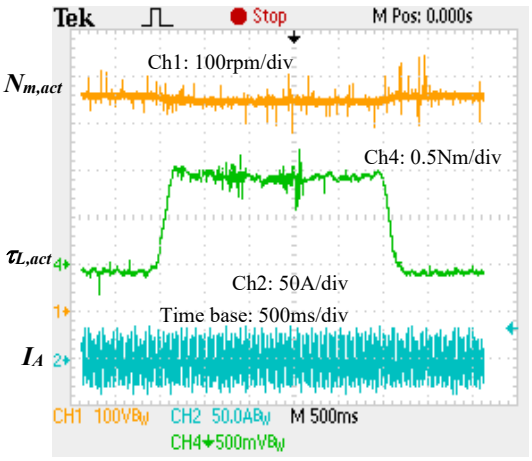

(c) Step load change on the motor

Fig. 13: *Dynamic performance of the open-loop speed control system with direct torque control.*

1 Nm-loaded and released. Clearly, the stator current of the BLDC remains the same during a suddenly applied load and released load, respectively. However, the motor speed slightly decreases during load conditions, as shown in Fig. 13(c).

5. CONCLUSION

This paper proposes the application of the DTC technique for a three-leg VSI, feeding a brushless DC motor. The open-loop DTC speed control is used. Clearly, the simulation and experimental results from the system's implementation on hardware demonstrate its capability in terms of reducing the spike from commutation and ripple on the voltage, current, stator flux linkage and electromechanical torque waveforms. In future work, the low-speed operation of the proposed DTC system for the BLDC could be improved with the use of a sophisticated stator flux linkage estimator and closed-loop speed control.

ACKNOWLEDGMENTS

This work was supported by the National Research Council of Thailand (NRCT) and the Faculty of Engineering, Rajamangala University of Technology Thanyaburi, Thailand, in 2019.

REFERENCES

[1] A. F. N. Azam, A. Jidin, N. A. Ngatiman, M. Jopri, M. Manap, A. L. Herlino, and N. F. Alias, "Current control of BLDC drives for EV application," in *2013 IEEE 7th International Power Engineering and Optimization Conference (PEOCO)*, Langkawi, Malaysia, 2013, pp. 411–416.

[2] K. Kamalapathi, P. V. Kumar, and C. Balaji, "Torque control of BLDC motor drive using MATLAB/SIMULINK," *International Journal of Emerging Trends in Engineering Research*, vol. 3, no. 6, pp. 448–452, 2015.

[3] H. F. Prasetyo, A. S. Rohman, F. I. Hariadi, and H. Hindersah, "Controls of BLDC motors in electric vehicle testing simulator," in *2016 6th International Conference on System Engineering and Technology (ICSET)*, Bandung, Indonesia, 2016, pp. 173–178.

[4] I. Takahashi and T. Noguchi, "A new quick-response and high-efficiency control strategy of an induction motor," *IEEE Transactions on Industry Applications*, vol. IA-22, no. 5, pp. 820–827, Sep./Oct. 1986.

[5] I. Takahashi and Y. Ohmori, "High-performance direct torque control of an induction motor," *IEEE Transactions on Industry Applications*, vol. 25, no. 2, pp. 257–264, Mar./Apr. 1989.

[6] M. Depenbrock, "Direct self-control (DSC) of inverter-fed induction machine," *IEEE Transactions on Power Electronics*, vol. 3, no. 4, pp. 420–429, Oct. 1988.

[7] D. Casadei, F. Profumo, G. Serra, and A. Tani, "FOC and DTC: two viable schemes for induction motors torque control," *IEEE Transactions on Power Electronics*, vol. 17, no. 5, pp. 779–787, Sep. 2002.

[8] Y. Chapuis, D. Roye, and J. Davoine, "Principles and implementation of direct torque control by stator flux orientation of an induction motor," in *Proceedings of 1995 IEEE Applied Power Electronics*

Conference and Exposition (APEC'95), 1995, pp. 185–191.

Sirichai Dangeam received his B.Eng. degree in electrical engineering from Rajamangala University of Technology Thanyaburi, Pathumtani, Thailand, in 1995, M.Eng. degree in electrical engineering from King Mongkut's University of Technology North Bangkok, Bangkok, Thailand, in 2003, and D.Eng. degree in electrical engineering at the King Mongkut's Institute of Technology Ladkrabang, Bangkok, Thailand. He is currently working as an assistant professor at the Department of Electrical Engineering, Faculty of Engineering, Rajamangala University of Technology Thanyaburi, Pathumtani, Thailand. His main research interests include power converters and electric drives.